A Magnetically Actuated Microscaffold Containing Mesenchymal Stem Cells for Articular Cartilage Repair

*Gwangjun Go, Jiwon Han, Jin Zhen, Shaohui Zheng, Ami Yoo, Mi-Jeong Jeon, Jong-Oh Park, and Sukho Park**

This study proposes a magnetically actuated microscaffold with the capability of targeted mesenchymal stem cell (MSC) delivery for articular cartilage regeneration. The microscaffold, as a 3D porous microbead, is divided into body and surface portions according to its materials and fabrication methods. The microscaffold body, which consists of poly(lactic-co-glycolic acid) (PLGA), is formed through water-in-oil-in-water emulsion templating, and its surface is coated with amine functionalized magnetic nanoparticles (MNPs) via amino bond formation. The porous PLGA structure of the microscaffold can assist in cell adhesion and migration, and the MNPs on the microscaffold can make it possible to steer using an electromagnetic actuation system that provides external magnetic fields for the 3D locomotion of the microscaffold. As a fundamental test of the magnetic response of the microscaffold, it is characterized in terms of the magnetization curve, velocity, and 3D locomotion of a single microscaffold. In addition, its function with a cargo of MSCs for cartilage regeneration is demonstrated from the proliferation, viability, and chondrogenic differentiation of D1 mouse MSCs that are cultured on the microscaffold. For the feasibility tests for cartilage repair, 2D/3D targeting of multiple microscaffolds with the MSCs is performed to demonstrate targeted stem cell delivery using the microscaffolds and their swarm motion.

1. Introduction

The onset of osteoarthritis (OA) has increased as our worldwide society ages; the World Health Organization (WHO) announced that 40% of people over the age of 70 worldwide are suffering from OA.[1] In addition, the WHO reported that incidences of knee and hip OA, as the 11th most frequent cause of disability, have increased steadily.[2] OA mainly occurs in knee and hip joints and accompanies local inflammation and pain due to the loss of articular cartilage or degenerative change. In particular, because OA after its mid-term stage inflicts damage or loss to articular cartilage, it is difficult to introduce a conservative treatment, such as an anti-inflammatory analgesic, hyaluronic acid treatments, or physical therapy. The damaged articular cartilage needs invasive surgery, including artificial joint transplants and marrow stimulating techniques (drilling and fracture).[2]

Recently, autologous cell-based therapy, which uses chondrocyte or mesenchymal stem cell (MSC), has attracted great interest in articular cartilage repair.[3–5] The autologous cell-based cartilage repair as biomedical treatment help to slow down OA rate of development and avoid partial and total joint replacement.[6] Especially, in autologous cell-based articular cartilage regeneration, a scaffold with a porous structure has been used to enhance adhesion and support of the cells.[7–12] The scaffold consists of biocompatible and biodegradable materials, such as synthetic or natural polymers. Thus, scaffolds implanted at the defect site can degrade and disappear within several months; additionally, cells inside the implanted scaffold can form adult tissue simultaneously with scaffold degradation. However, in the case of millimeter- and centimeter-scale scaffolds, their implantation requires a surgical operation including a fixation process (i.e., suture, fibrin glue) to secure the scaffold.[7,8] In addition, scaffolds on the scale of millimeters can lead to cell necrosis in the center owing to the difficulty of nutrient/oxygen supply and metabolic waste transportation.[13] Alternatively, microscale scaffolds containing cells can approach to the joint cavity through needle-based injection.[9–12] Although needle-based injection clearly avoids invasive surgery, including incision, the injected microscaffolds might be dispersed in the joint cavity due to the absence of active locomotion of the microscaffolds.[14] Therefore, to treat damaged cartilage, large amounts of cell-loaded scaffolds should be delivered to the joint cavity with the cartilage defect.

To overcome the shortcomings of cell-based cartilage repair, cells, or scaffolds with the capability of magnetic actuation have been studied for active targeting and fixation to the lesions.[15–19] For cells or scaffolds with magnetic behavior,

G. Go, Dr. J. Han, J. Zhen, S. Zheng, A. Yoo, M.-J. Jeon, Prof. J.-O. Park
Medical Microrobot Center (MRC)
Robot Research Initiative (RRI)
Chonnam National University
Gwangju 500-480, South Korea
G. Go, J. Zhen, S. Zheng, Prof. J.-O. Park, Prof. S. Park
School of Mechanical Systems Engineering
Chonnam National University
Gwangju 500-757, South Korea
E-mail: shpark12@dgist.ac.kr
Prof. S. Park
Department of Robotics Engineering
Daegu Gyeongbuk Institute of Science and Technology
Daegu 711-873, South Korea

DOI: 10.1002/adhm.201601378

© 2017 WILEY-VCH Verlag GmbH & Co. KGaA, Weinheim

magnetic nanoparticles (MNPs) under 50 nm were adopted, where MNPs have high effective surface areas for easier attachment of ligands and can label specific biomolecules or living cells.[20,21] In addition, MNPs are also incorporated into iron store into the body through metabolism in the lysosome.[22] However, the proposed MNP-loaded cells or scaffolds can have drawbacks, such as inaccurate targeting by the control limit of the external magnetic field generation system or invasive surgery from the transplantation of the magnetic generation device. For example, Mahmoud et al. proposed MNP-loaded MSCs, which were guided to medial patella lesions in a rabbit model using external magnetic fields generated in a superconducting magnet system.[18] However, because the MSCs are propelled along only one magnet orientation, it is difficult for them to be accurately guided to cartilaginous defects located in the patellofemoral groove. Additionally, the MSCs far away from the magnet system are difficult to move quickly due to small amounts of MNPs loaded in the MSCs with microscale. Next, Panseri et al. reported that a collagen-based scaffold containing ferromagnetic fluid or MNPs was magnetically pulled to the defect site through four permanent magnets that were implanted in the lateral condyle of the rabbit model.[19] However, this approach for cartilage repair requires invasive surgical operations, such as implantation and removal of the permanent magnets before and after cartilage regeneration procedure.

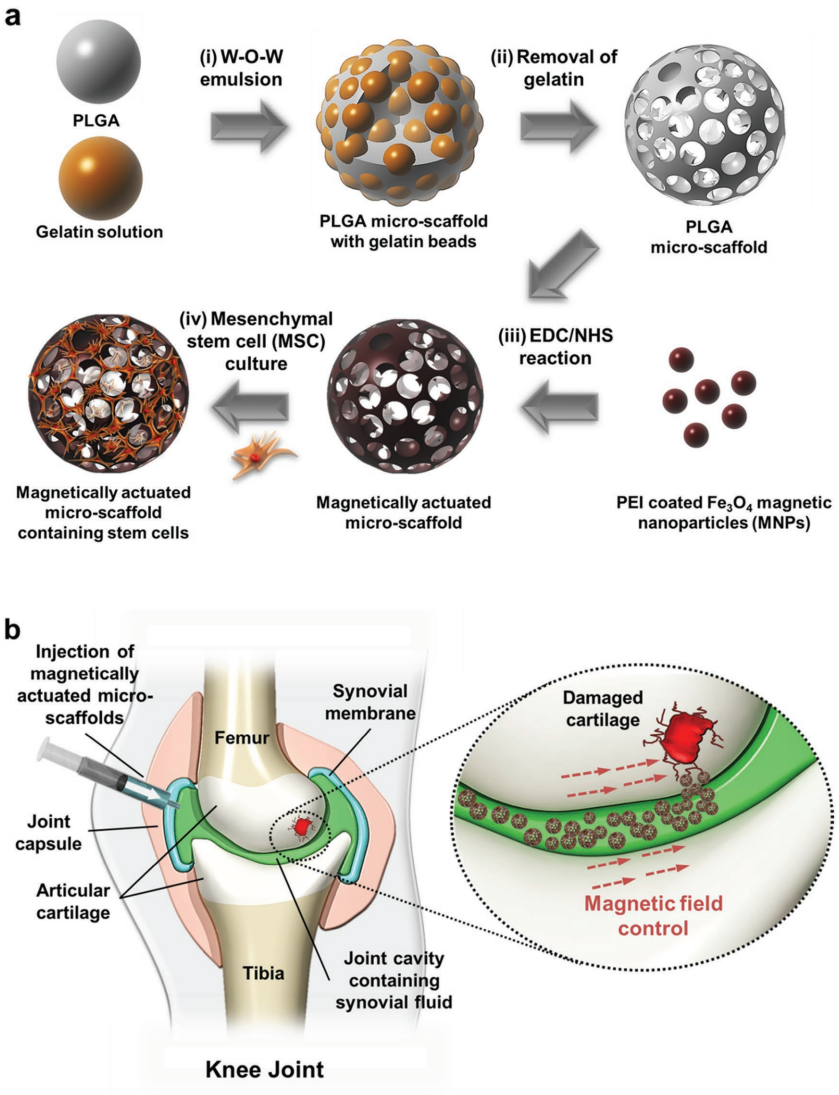

Figure 1. Concept of the magnetically actuated microscaffolds for targeted stem cell delivery. a) Schematic diagram of the fabrication process: (i) W-O-W emulsion, (ii) removal of gelatin, and (iii) amino bond formation. After fabrication, MSCs were cultured on the magnetically actuated microscaffold ((iv) MSC culture). b) Schematic diagram of articular cartilage repair using the magnetically actuated microscaffold.

This paper proposes a magnetically actuated microscaffold carrying MSCs for articular cartilage regeneration. The microscaffold is a 3D porous microbead that is designed to not only support the adhesion and migration of MSCs but also be guided to a target site through the driving capability of external magnetic fields. The body and surface of the microscaffold consist of poly(lactic-co-glycolic acid) (PLGA) as a biocompatible and biodegradable polymer and MNPs with superparamagnetic behavior, respectively (**Figure 1**a). The body of the 3D porous PLGA microscaffold is obtained via water-in-oil-in-water (W-O-W) emulsion and gelatin particulate leaching. Afterwards, the PLGA microscaffold is covered with polyethylenimine (PEI)-coated Fe_3O_4 MNPs through an *N*-hydroxysuccinimide/ethyl(dimethylaminopropyl) carbodiimide reaction. First, the magnetic actuation performance of the microscaffold was characterized with respect to the magnetization curve and the magnetic actuation response using a permanent magnet. We also tested the moving velocity and 3D locomotion of a single microscaffold using an external electromagnetic actuation (EMA) system and evaluated the 2D/3D targeting feasibility of multiple microscaffolds. In addition, the cell support/adhesion/culture capability of the microscaffold was demonstrated through the proliferation, viability, and chondrogenic differentiation of D1 mouse MSCs, which were seeded and cultivated in the microscaffold. Compared with the current articular cartilage therapy, such as artificial joint implants and stimulating techniques using drilling and microfracture, the proposed prototype using microscaffolds carrying MSCs provides targeted stem cell delivery with minimally or noninvasive surgery via a needle-based injection into synovial fluid (Figure 1b). For a knee joint, microscaffolds containing MSCs can be injected into the joint cavity through the needle of a syringe and then moved to the site of damaged cartilage using external magnetic fields.

© 2017 WILEY-VCH Verlag GmbH & Co. KGaA, Weinheim

2. Results and Discussion

2.1. Fabrication of the Magnetically Actuated Microscaffold

The magnetically actuated microscaffold, which consists of a PLGA porous body and Fe_3O_4 MNPs attached to the surface, was fabricated by the emulsion templating method and protein coupling using amino bond formation. The detailed fabrication process of the magnetic actuated microscaffold is presented in the Supporting Information. First, the PLGA microscaffold with gelatin beads was obtained by double emulsion with a fluidic device (Figure 1ai). After the formation of W-O-W droplets, the gelatin beads within the PLGA microscaffold were removed (Figure 1aii). In this process, it is important to obtain a PLGA microscaffold with stable morphology because various factors of porous scaffolds, such as surface openness, interconnectivity of inner pores, porosity, and size uniformity can influence MSC proliferation and differentiation. To find the proper morphology of the PLGA microscaffold, we observed the PLGA microscaffolds and measured their porosity according to the volume (0.55–0.85 mL, 0.1 mL interval) of the gelatin solution (Figure S1, Supporting Information). As a result, the PLGA microscaffolds using a small volume (0.55 mL) of gelatin solution have low porosity of 42.88 ± 12.97% and narrow surface openness in Figure S1a in the Supporting Information, and thus they are not suitable for MSCs seeding. In addition, the PLGA microscaffolds using high volumes (0.75 and 0.85 mL) have high porosity of 67.75%, but unstable morphologies, as shown in Figure S1c,d in the Supporting Information. Therefore, we selected 0.65 mL of the gelatin solution as the optimum volume for the proposed PLGA microscaffolds. As shown in scanning electron microscopy (SEM) images (**Figure 2**a), the PLGA microscaffold using the optimal volume of the gelatin solution has microbead morphologies such as the outer diameters of 269.83 ± 10.982 μm and the surface pores of 37.68 ± 7.55 μm (Figure S2a,b, Supporting Information). In addition, through the cryosectional images of the microscaffolds, we observed that they have inner pores of 40.12 ± 7.45 μm in diameter (Figure S2c, Supporting Information). We expected that the larger inner pore size relative to the surface pores was caused by the aggregation of several gelatin droplets during the W-O-W emulsion process. The fabricated microscaffolds satisfy the conditions of porous scaffold beads as a cell carrier, where the conditions dictate a bead diameter in the range of 100–500 μm and pores sizes over 20 μm.[14] Furthermore, the large surface openness and high interconnectivity of the microscaffold can help the transportation of nutrients and oxygen and the cell migration in the microscaffold.

Next, to endow magnetic actuation to the PLGA microscaffold, amine-functionalized MNPs, which are composed of a nanoscale Fe_3O_4 core and a PEI-coated surface, were chemically bonded by protein coupling to the surface of the PLGA microscaffold (Figure 1aiii). Figure 2b shows the SEM images and energy dispersive X-ray spectrometry (EDX) maps for the PLGA microscaffold with amine-functionalized MNPs. In SEM images of the PLGA microscaffold and the MNP-attached PLGA microscaffold, the presence of the micropores and the MNPs was verified based on the surface morphology. Additionally, through the EDX maps of the magnetically actuated microscaffold, the C, O, and Fe signals confirm the presence of PLGA and MNPs. Compared with the PLGA microscaffold, there were no significant changes to the outer diameter and the pore diameters in the MNPs attached microscaffold because the MNPs were thinly distributed on the surface of the PLGA microscaffold.

2.2. Characterization of the Magnetically Actuated Microscaffold

The magnetically actuated microscaffold was characterized through various basic tests, such as the magnetization curve,

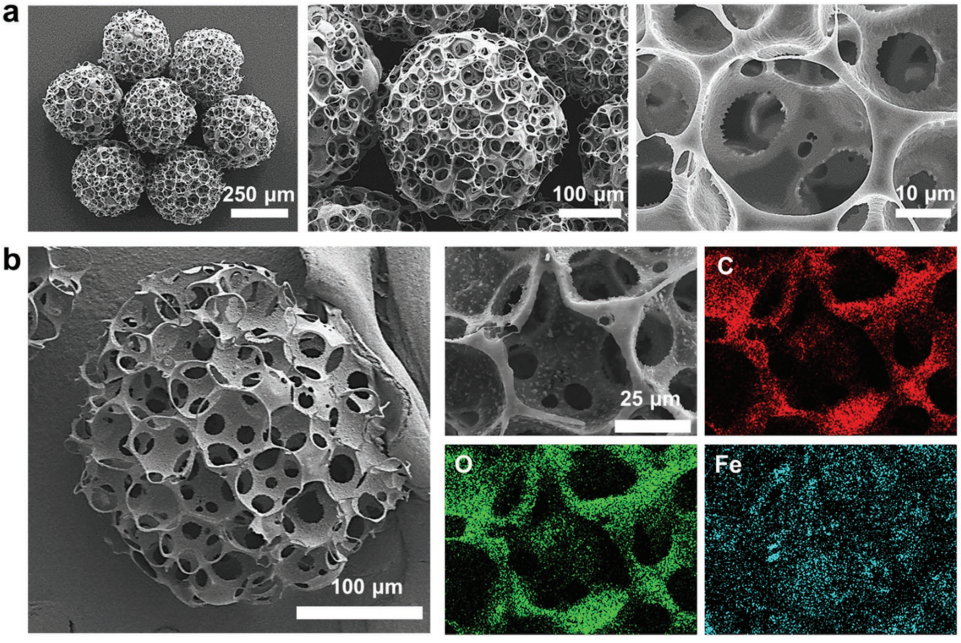

Figure 2. a) An SEM image (left) of the PLGA microscaffolds after W-O-W emulsion templating with 0.65 mL gelatin solution, with enlarged images (middle and right). b) An SEM image (left) and EDX maps (right) of a magnetically actuated microscaffold after the MNP attachment process.

© 2017 WILEY-VCH Verlag GmbH & Co. KGaA, Weinheim

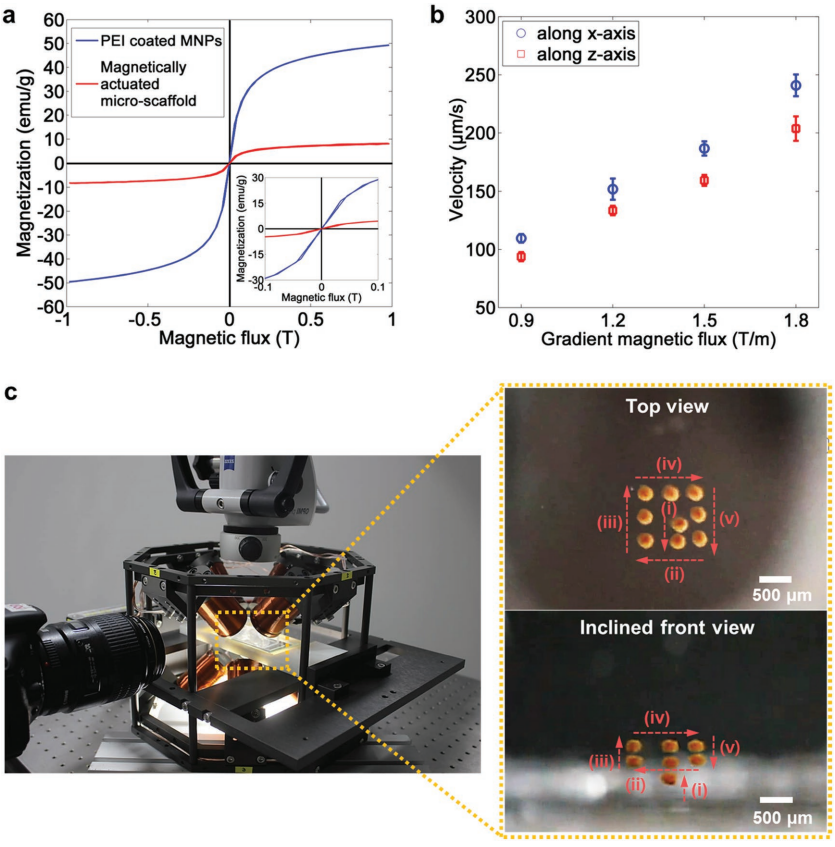

Figure 3. Characterization of the magnetically actuated microscaffold. a) Magnetic hysteresis of the MNP-attached microscaffold and PEI-coated MNPs. b) Velocity of the microscaffold along the *x*- and *z*-axes ($n > 3$). c) 3D locomotion of a single microscaffold using an EMA system integrated with the operating microscope and an inclined DSLR camera. (i) Levitation of the microscaffold along *z*-axis; (ii)–(v) Locomotion of the microscaffold along rectangular path on the *x*–*y* plane.

the magnetic actuation response using a permanent magnet, moving velocity and 3D locomotion of a single microscaffold using the EMA system. First, the magnetically responsive property of the microscaffold was measured through the magnetization curve using a vibrating sample magnetometer (VSM), which generates external magnetic fields ranging from −1 to 1 T at room temperature. The magnetization curve of the microscaffold showed a magnetic hysteresis loop with a saturation magnetization of 8.105 emu g^{-1} and near-zero coercivity (**Figure 3**a), indicating that the microscaffold had one-fifth of the saturating magnetization of the PEI-coated MNPs and similar superparamagnetic behavior without residual magnetism.

Second, the basic magnetic actuation test of the microscaffolds was performed using a permanent magnet (Figure S3 and Video S1, Supporting Information). With no exposure to a magnetic field, the microscaffolds dispersed in the deionized water dropped downward due to gravitational force. With the approach of the permanent magnet, the microscaffolds were attracted by external magnetic fields. When the permanent magnet was moved far from the microscaffolds, they sank to the bottom. Then, the microscaffolds could be dispersed again through physical shaking. Through this test result, we confirmed that the magnetically responsive microscaffolds could move along the direction of the gradient magnetic fields as a group.

Third, for the manipulation of the microscaffold in 3D space, we introduced an EMA system, which is composed of eight coils with pure iron cores. The EMA system not only provides a magnetic gradient pulling motion to the microscaffold but also compensates for the gravitational force on the microscaffold. Through the control of the magnetic fields generated by the eight coils, the microscaffold can be stably manipulated in 3D space. Generally, because the synovial fluid in the joint cavity of the normal human body has high viscosity, the microscaffolds cannot freely move by a high fluid drag force in the normal synovial fluid.[23] However, in the damaged joint, it is reported that the viscosity of the synovial fluid decreases to the range of 20–30 cP by an inflammatory reaction around the cartilage defects.[24] Thus, we adopted a glycerin (70% (v/v)) solution at room temperature (25–26 °C), which has a similar viscosity to the synovial fluid in a joint with inflammatory disease (Figure S4, Supporting Information). Using the EMA system and the glycerin solution, we measured the moving velocities of the microscaffold according to the generated magnetic fields. Figure 3b shows that the moving velocities of the microscaffold along the *x*- and *z*-axes linearly increased according to the fixed uniform magnetic field (45 mT) and the varying gradient magnetic fields (0.9–1.8 T m^{-1}, interval 0.3 T m^{-1}) by the EMA system. And, to confirm the mobility of the microscaffold with different viscosity values, we measured its velocities at various glycerol solutions (70%–85% (v/v), interval 5% (v/v)) (Figure S5, Supporting Information). As the viscosity of the glycerol solutions increased, the moving velocity proportionally decreased. In addition, the microscaffold has the lower moving velocity along *z*-axis rather than *x*-axis, which means that the gravitational force on the microscaffold can be attributed.

Finally, we demonstrated a teleoperated manipulation of a single microscaffold in 3D space (Figure 3c and Video S2, Supporting Information). As shown on the left of Figure 3c, to observe the 3D locomotion of the microscaffold, an inclined digital single lens reflex (DSLR) camera and an operating microscope were installed in the EMA system. Once the microscaffold was positioned at the surface of the container filled with the glycerin solution, the uniform magnetic field and the gradient magnetic field were applied in the *z*-axis to levitate the microscaffold (Figure 3c-right i). After its levitation, the presence of the gravitational force and the fluid flow acting on the microscaffold was checked by the EMA system. Then, the microscaffold was moved again along the *z*-axis and steered along the rectangular path on the *xy*-plane through the gravity compensation of the EMA system (Figure 3c-right ii–v). Lastly,

© 2017 WILEY-VCH Verlag GmbH & Co. KGaA, Weinheim

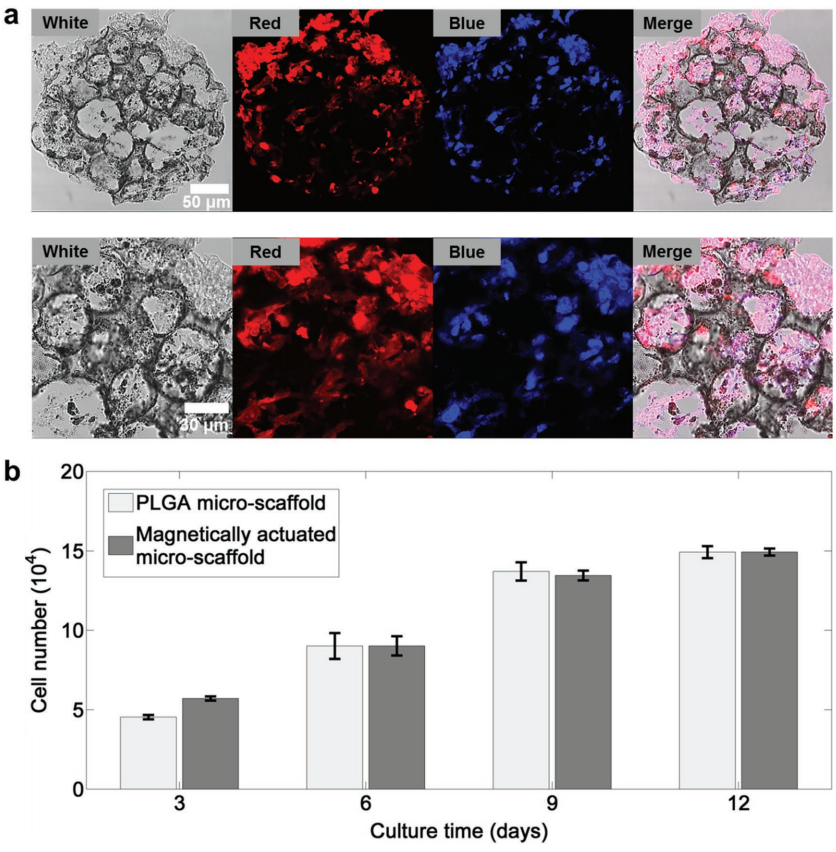

Figure 4. a) A confocal image (top) of MNP-attached microscaffolds containing MSCs after culturing for 5 d, with an enlarged image (bottom). Red and blue colors in the images were obtained after cytoplasmic and nuclear staining, respectively. b) MSCs proliferation and viability on the microscaffolds (PLGA microscaffold and MNP-attached microscaffold) by AlamarBlue assay after cell seeding on scaffolds for 3, 6, 9, and 12 d.

the microscaffold was manipulated to the initial position. From the 3D manipulation test, we confirmed that the microscaffold can freely move in the 3D space by the external magnetic fields generated in the EMA system.

2.3. MSC Proliferation, Viability, and Differentiation in the Microscaffold

We adopted D1 mouse MSCs to verify the proliferation, viability, and differentiation of MSCs cultured in the microscaffolds. The MSCs and the microscaffolds were co-cultured up to day 12 in cell culture medium containing fetal bovine serum (FBS) (Figure 1aiv). A number of the MSCs existed inside the microscaffold and on its outer surface (**Figure 4**a). In particular, we confirmed that the MSCs were attached to the inner wall of the microscaffold (Figure S6, Supporting Information). Through a quantitative cell proliferation assay, in the PLGA microscaffolds and the magnetically actuated microscaffolds (the PLGA microscaffold with MNPs), the MSCs showed similar viability and growth patterns, with a significant increment in cell quantities from day 3 to day 9 (Figure 4b). At day 9, significant increases of the MSCs (2.5-fold increase), in comparison with the cell numbers at day 3, showed in both types of microscaffolds. Additionally, at 3 d of culture, the number of MSCs inside the MNP-attached microscaffold was higher over 26% than the PLGA microscaffold.

Next, we evaluated the chondrogenic differentiation of the MSCs in the PLGA microscaffolds and the magnetically actuated microscaffolds by Alcian blue staining of cartilage aggrecan,[25] collagen type II antibody staining, and quantitative real-time reverse-transcription polymerase chain reaction (qRT-PCR) of chondrogenic marker genes such as *Aggrecan* (*AGG*), *COL2A1*, and *SOX9*.[26,27] The MSCs cultured in both types of microscaffolds, which were grown in an appropriate chondrogenic medium over 21 d, were stained with Alcian blue by proteoglycans synthesis (**Figure 5**a,b and Figure S7, Supporting Information) and collagen type II antibody (Figure S8, Supporting Information). Moreover, we found that the gene expression level of the chondrogenic marker genes *AGG*, *COL2A1*, and *SOX9* were also highly expressed (Figure 5c).

2.4. 2D and 3D Targeting Tests

As feasibility tests for articular cartilage repair, we demonstrated 2D and 3D targeting of multiple microscaffolds using the magnetic guidance of the EMA system. First, the 2D targeting test was performed to show a targeted stem cell delivery using the magnetically actuated microscaffolds (**Figure 6**a–c and Video S3, Supporting Information). Prior to this test, the microscaffolds were cultivated with MSCs over 5 d, and the cytoplasms of the cells were stained for fluorescence assays. Then, ten microscaffolds containing the MSCs were injected along with culture medium into the loading area of a test chamber. The test chamber was fabricated through a general molding technique using polydimethylsiloxane (PDMS) and was divided into control, loading, and target areas. The microscaffolds loaded in the test chamber were placed in the workspace of the EMA system integrated with an inverted microscope, which enables the observation of both the optical image of the microscaffolds containing the MSCs and the fluorescence image of the D1 MSCs in the microscaffolds. In the initial state, the optical and fluorescence images show the microscaffolds and the presence of the MSCs on the microscaffolds, respectively (middle of Figure 6a and left of Figure 6c). Subsequently, the microscaffolds containing the MSCs were magnetically guided to the target area by the magnetic field control. As shown in Figure 6c, there was no loss of the MSCs from the microscaffolds during the magnetic guidance. Additionally, the microscaffolds moved at different speeds due to their surface frictional forces, and one among the ten microscaffolds failed the targeted cell delivery.[28] The 2D targeting test was repeated five times to obtain the statistical result of

© 2017 WILEY-VCH Verlag GmbH & Co. KGaA, Weinheim

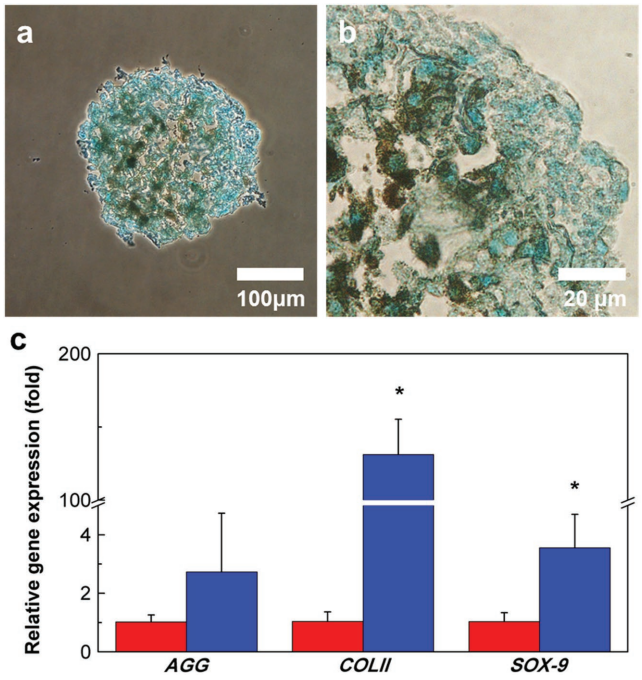

Figure 5. a,b) Optical micrographs of a cryosectioned MNP-attached microscaffold containing the Alcian blue-stained MSCs, c) Expression of cartilage-specific genes, *AGG*, *COL2A1*, and *SOX9* after 21 d of incubation in chondrogenic differentiation medium.

the 2D targeting test. As a result, only two in thirty microscaffolds failed the targeted MSC delivery on the surface of the 2D plane. In this test, we expected that the targeting accuracy of the microscaffold can be improved in 3D space because the surface frictional force can be neglected.

Next, to verify the targeting feasibility of the magnetically actuated microscaffolds to an articular cartilage defect, we performed a magnetic manipulation of the microscaffolds in a 3D knee joint phantom (Figure 6d,e and Video S4, Supporting Information). As shown in Figure 6d, the phantom was fabricated by a 3D printer, and the target area was created in the medial condyle of the femur in the knee joint phantom. The phantom was fixed on the container filled with the glycerin solution. Then, five microscaffolds were loaded into the intra-articular cartilage of the knee joint phantom and manipulated to the target area through the magnetic fields of the EMA system. Figure 6a and Video S4 in the Supporting Information show that the five microscaffolds were moved from the injection point to the target area with similar velocities. Consequently, through these results on the 2D/3D targeting tests, we expected that the magnetically actuated microscaffold will be used for targeted stem cell delivery through the EMA system.

2.5. Discussion

In this study, we proposed a magnetically actuated microscaffold containing MSCs for cartilage repair. To mimic the properties of natural 3D extracellular matrix, we fabricated a biocompatible and biodegradable PLGA microscaffold. Additionally, PEI coated MNPs were attached to the surface of the PLGA microscaffold for targeted stem cell delivery using magnetic actuation. As basic fundamental tests, we analyzed characterization of the microscaffold through magnetization value and moving velocity of the microscaffold. In addition, the ability of MSCs to proliferate and differentiate in the microscaffold was investigated. Finally, we confirmed the feasibility of the proposed microscaffolds by 2D/3D targeting test. However, for in vivo application on a cartilage repair, we should consider additional factors, such as the adhesion of the microscaffold to the normal articular surface and the viscosity change of synovial fluid according to lesion status, which can affect the locomotion of the microscaffolds containing MSCs using the EMA system.

First of all, the debris formed by degraded tissue in an osteoarthritic joint can affect the locomotion of the microscaffold. When the size of the debris is smaller than the microscaffold, we expected that the microscaffold can move in synovial fluid without serious disturbance by debris. However, when the debris is larger than the microscaffold, it can be an obstacle for the microscaffold to be steered to cartilage defect. As an alternative, arthroscopic lavage and debridement can be applied to remove the debris.[29] Through this procedure before injection of the microscaffolds, we cannot only remove the debris and but also clearly observe the image of microscaffolds using arthroscopy or X-ray.

In 3D targeting test, we used a glycerin solution of 20–30 cP to mimic inflamed synovial fluid. However, Jebens et al. reported that the viscosity of synovial fluid in OA knee joint was 80 cP.[23] Therefore, we need to consider the moving velocity of the microscaffold in the synovial fluid with high viscosity. In the locomotion of a single microscaffold in 3D space, the dynamics of the microscaffold with a uniform velocity can be modeled as

$$F_{\text{mag}} - F_{\text{drag}} - F_{\text{gravity}} = 0 \tag{1}$$

where F_{mag}, F_{drag}, and F_{gravity} are the magnetic force, fluidic drag force, and gravitational force acting on the microscaffold, respectively.[30] When the size of the microscaffold and the magnetic field generated in EMA system are fixed, the gravitational force (F_{gravity}) and the magnetic force (F_{mag}) are constant, and thus the fluidic drag force (F_{drag}) is also constant. Based on the spherical microscaffold, the drag force of a spherical object with a low Reynolds number can be expressed as

$$F_{\text{drag}} \cong 6\pi\mu RV \tag{2}$$

where R, V, and μ are the radius and moving velocity of the microscaffold and the coefficient of viscosity, respectively.[31] When the fluidic drag force (F_{drag}) and the radius (R) of the microscaffold are constant, the velocity of the microscaffold is inversely proportional to the viscosity of the synovial fluid. Therefore, we expected that the moving velocity of the microscaffold at a high viscous fluid (80 cP) will be reduced to one quarter of that of the microscaffold at a low viscous fluid (20 cP). In the velocity measurement test (Figure S5, Supporting Information), we confirmed that the moving velocity of the microscaffold proportionally decreased as the viscosity of the glycerol solution increased. In addition, if we want to generate higher

© 2017 WILEY-VCH Verlag GmbH & Co. KGaA, Weinheim

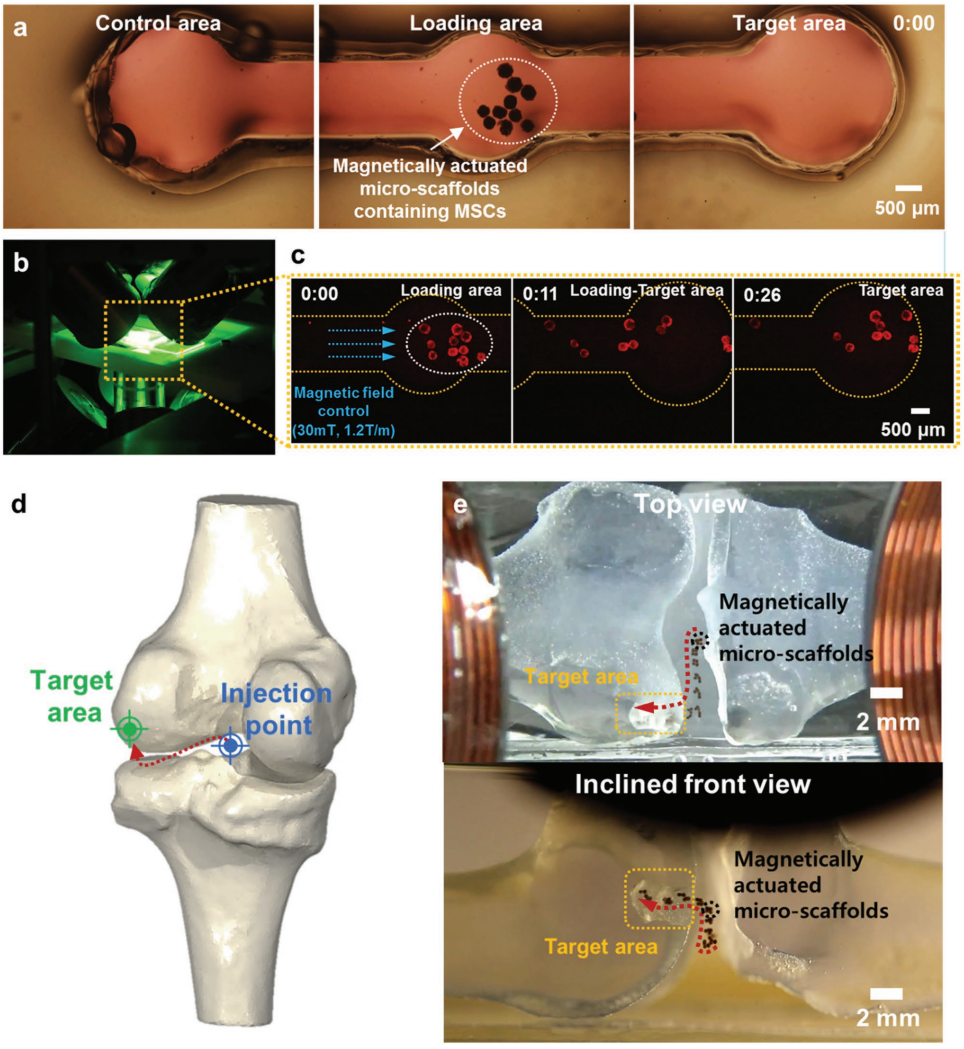

Figure 6. 2D and 3D targeting tests of the magnetically actuated microscaffolds. In the 2D targeting test: a) Optical images of a PDMS chamber and the microscaffolds containing MSCs in the initial state. b) EMA system integrated with an inverted microscope. c) Fluorescence images of microscaffolds containing MSCs during magnetic guidance to the target area. The time is indicated on each figure in the minutes:seconds format. In the 3D targeting test: d) A 3D model of a knee joint showing the injection point and the target area. e) Time-lapse images of the magnetically actuated microscaffolds during targeting using the EMA system. Arrow with red dashed line indicates the path of the microscaffolds.

moving velocity of the microscaffold, EMA system could be enhanced to generate higher magnetic field.

In the proliferation and viability results, the MSCs aggregated and maintained 3D structures in the two microscaffold groups (PLGA microscaffold and MNP-attached microscaffold) with highly proliferative properties up to at least 12 d, with no cytotoxic effects due to the MNPs. First, generally, because PLGA has negative charge, the cell with negatively charged cell membrane is difficult to adhere on the surface of the PLGA microscaffolds.[32,33] However, because D1 cells were cultured with the PLGA microscaffolds in a cell culture medium including FBS, the specific proteins in the FBS were absorbed into the surface of the PLGA microscaffolds and the D1 cell attachment was promoted through integrin receptors.[34,35] Next, in MNP-attached microscaffolds, the use of positively charged PEI-MNPs enables cells attachment to the microscaffold.[36,37] The PEI as a cationic polymer can facilitate attachment between cell membrane and microscaffold. Thus, the D1 cells are attracted and adhered to the MNP-attached PLGA microscaffold. Consequently, D1 cell can adhere on PLGA microscaffold and PEI coated PLGA microscaffold and there are no significant differences in the viability test. In addition, at 3 d of culture, the number of MSCs inside the MNP-attached microscaffold was higher over 26% than the PLGA microscaffold. However, after 6 d of culture, the number of MSCs in the MNP-attached microscaffold was almost the same as that in the PLGA microscaffold. Therefore, at the initial culture time, we expected that the negatively charged cell membrane of D1 cell could strongly interact with the positively charged MNP-attached microscaffold.

It is important to know the acceptable dose of MNPs in human body because high concentration of MNPs can potentially cause a toxic side effect. The acceptable dose of MNPs for articular cartilage has not been determined yet. Alternatively, based on the dose of MNPs used for MRI contrast, a small

© 2017 WILEY-VCH Verlag GmbH & Co. KGaA, Weinheim

MNPs dose (≈50–200 mg per person) is administered, in comparison with total body iron stores (≈4000 mg in a normal male adult).[38] Using the dose of MNPs for MRI contrast (125 mg) and the weight of MNPs in the magnetically actuated microscaffold (≈0.133 μg), we estimated that ≈9.40×10^5 can be injected into the articular cartilage in toxicity aspect. However, the proposed MNPs attached microscaffold is required to be magnetically targeted to articular cartilage defect. Thus, high concentration of MNPs accumulated in localized area can lead to toxic implications such as DNA damage, oxidative stress, and inflammation.[39] In the future work, the toxicity due to the accumulation of MNPs in a localized area will be confirmed through in vivo test.

Additionally, chondrogenic differentiation of the MSCs on the two types of microscaffolds was achieved in chondrogenic medium including transforming growth factor-β1 (TGF-β1). Chondrogenic nature of the MSCs in both types of microscaffolds were demonstrated by aggrecan staining, cartilage collagen II staining, and qRT-PCR of chondrogenic marker genes, and showed similar chondrogenic differentiation capability.

As feasibility tests of our work, we conducted 2D/3D targeting tests using magnetically controlled manipulation of the microscaffolds by the EMA system. However, in vivo models, large number of microscaffolds should be injected and manipulated into joint cavity to fill the cartilage defect. Therefore, we need to know how many microscaffolds are required to treat cartilage defect of human or animal. In clinical test, the cartilage treatment method is determined by the location and lesion size of cartilage defect, where the standard lesion size is average 2.5×2.5 cm^2.[40] Based on this average cartilage defect size, about 8.57×10^3 microscaffolds should be injected into the joint cavity. Therefore, the number of the microscaffolds can be determined by the size of cartilage defect. In addition, microscaffolds can be injected into the joint cavity and then can be moved freely to the desired direction in synovial fluid through magnetic field generated by the EMA system. However, the EMA system used in this work can generate magnetic field along same direction in the workspace. Hence, the microscaffolds spreading in synovial fluid can only move in the same direction and cannot be manipulated individually. Therefore, contrary to manipulating a small number of microscaffolds, it is difficult to delivery numerous microscaffolds to cartilage defect. As an alternative, if microscaffolds were injected in front of the target and at the same time a magnetic field was generated along the target direction, most microscaffolds can move to the target lesion. Through this microscaffold targeting strategy, we expect to be able to transport microscaffolds to cartilage defect by a single injection.

Despite the powerful performance and functionality of the proposed magnetically actuated microscaffolds, several considerations should be addressed in a clinical application for an articular cartilage repair. First, TGF-β1 as a growth factor is an important element for the chondrogenic differentiation of MSCs from in vitro and in vivo environments. In an in vivo application for cartilage repair, TGF-β1 is injected into the joint cavity and spread to the whole of the articular cartilage, including the damaged area. Thus, compared with the required amount of treatment for a target lesion, a high amount of free TGF-β1 can lead to severe side effects, such as osteophyte formation.[41] Therefore, in the future, we plan to study microscaffolds containing the proper amounts of TGF-β1, MNPs, and MSCs for cartilage regeneration. Second, some studies mentioned that the cartilage regenerated by autologous MSCs implantation is very thin and thus not similar to mature cartilage tissue, and the hypertrophy of cartilage by MSCs implantation can cause the ossification of normal cartilage tissue.[42,43] Recently, it was reported that the co-culture of chondrocyte and MSCs can be used for articular cartilage defect to solve the problems of conventional MSCs implantation.[44,45] Therefore, in a future study, we will conduct an experiment in which MSCs and chondrocyte are co-cultivated in a scaffold. Third, we observed the position of the microscaffolds using optical methods, such as microscopes and a DSLR camera in real time. However, for in vivo applications, a different position recognition method should be adopted because microscaffolds injected into the synovial fluid of a joint cavity cannot be tracked using optical methods. As an alternative candidate, an arthroscope, which observes the insides of the knee and hip joints with small incision through the skin and other tissues, can be applied to view the microscaffolds in real time. In addition, an X-ray fluoroscope can be adopted in the tracking of the microscaffolds. Fourth, after the targeting process using the EMA system, the microscaffolds containing MSCs need to be fixed to the cartilage defects during the patient's recovery period. However, the EMA system is temporarily operated only for the targeting process of the microscaffolds because the EMA system generally has a large volume and needs a high power supply for the procedure. As a solution, a wearable magnetic actuation device, which consists of an array of permanent magnets and a supporting frame, can be applied to maintain the delivered microscaffolds. The magnets of the wearable device can be arranged according to the position and shape of the target lesion, and the generated magnetic fields in the wearable device can help securely fix the microscaffolds to the target lesion. Of course, the wearable device should not be taken off during treatment period because the microscaffolds that are not fully connected to the cartilage defect might be detached from the targeted area due to external impact. In addition, there are studies that show that continuous static magnetic field exposure can assist chondrogenic differentiation and chondrocyte cell growth of MSCs.[46,47] Therefore, we expect that the magnetically actuated microscaffolds containing MSCs can be applied to clinical articular cartilage repair, as shown in Figure S9 of the Supporting Information; in the case of the knee joint, the microscaffolds containing MSCs are injected into the joint cavity in an arthroscopic surgery via a minimal incision and are then magnetically steered to the cartilage defect through real-time imaging using the arthroscope or X-ray microscope. After the targeting process of the microscaffolds containing MSCs, a wearable magnetic device is applied to fix the microscaffolds to the lesion. In future work, we will introduce the cartilage repair process to in vitro and in vivo testing.

3. Conclusion

In summary, we have reported the development of magnetically actuated microscaffolds containing MSCs for articular

© 2017 WILEY-VCH Verlag GmbH & Co. KGaA, Weinheim

cartilage regeneration. The microscaffold as a targeting cargo of MSCs consists of a biocompatible and biodegradable PLGA porous body with an MNP-coated surface capable of magnetic actuation using external magnetic fields. The magnetic actuation performance of the microscaffold was evaluated through the magnetization curve, moving velocity, and 3D locomotion of a single microscaffold. In addition, its role as a cell container was verified based on the proliferation, viability, and chondrogenic differentiation of MSCs that were cultured on the microscaffold. Finally, as feasibility tests for the application to cartilage repair, we performed 2D/3D targeting of the microscaffolds, in which the microscaffolds containing MSCs can be magnetically guided to the target area. Through the results of this work, we expect that magnetically actuated microscaffolds carrying MSCs have great potential for applications in articular cartilage regeneration.

4. Experimental Section

A detailed description of the fabrication of the magnetic actuated microscaffold can be found in the Supporting Information.

Experimental Setup for Magnetic Actuation Control: For the magnetic actuation of MNPs attached to microscaffolds in 3D space, the EMA system, which is composed of eight electromagnetic coils and pure iron cores (JL Magnet, South Korea), was introduced (Figures S10 and S11a, Supporting Information). Through the current control of the eight coils, the EMA system can simultaneously produce uniform magnetic fields and gradient magnetic fields up to 45 mT and 1.8 T m^{-1} and can also realize the wireless locomotion of magnetic objects with five degrees of freedom.[48,49] In addition, through the integration of an operating microscope (f170, Carl Zeiss, Germany), a DSLR camera (EOS 600D, CANON, Japan), and an inverted microscope (Eclipse Ti-U, Nikon, Japan) with the EMA system, one can observe optical images and fluorescence images of the microscaffolds containing D1 MSCs in real time. The locomotive control of the microscaffolds using the EMA system was performed by a joystick and a PC with LabVIEW software (National Instruments, Austin, Texas, USA), where they were used for the locomotive control of the microscaffold and the input current control of the eight coils, respectively. The input currents of the coils were applied by eight power supplies (each four sets of MX 15 and 3001 ix, AMETEK, USA).

Characterization of the Magnetically Actuated Microscaffold: The morphologies of the PLGA microscaffold and the MNP-attached microscaffold were observed using an SEM (SU8010, HITACHI, Japan). The C/O/Fe signals in the MNPs attached to the microscaffolds were also investigated using EDX.

Based on the SEM images, the surface porosity of the PLGA microscaffold according to the gelatin solution (0.55–0.85 mL, interval 0.1 mL) for each 20 samples of the PLGA microscaffolds were measured using ImageJ software (National Institutes of Health, USA). Similarly, the PLGA microscaffolds using the optimal volume of gelatin solution (0.65 mL) were fabricated, and the SEM images of 48 PLGA microscaffolds were used to measure the outer diameters and surface pore sizes and the cryo-sectioned SEM images of 8 PLGA microscaffolds were used to measure the inner pore sizes.

The magnetization property of the MNP-attached microscaffolds was evaluated by recording a magnetic hysteresis loop of samples, which was measured using VSM (Lake Shore 7404, Lake Shore Cryotronics, USA).

The basic magnetic actuation of the MNPs attached to the microscaffolds immersed in the deionized water was tested using a permanent magnet. The permanent magnet consisted of four cylindrical neodymium magnets (diameter 10 mm × height 20 mm) with 955 kA m^{-1} of magnetization value.

Materials for MSC Proliferation, Viability, and Cell Differentiation: For the proliferation, viability, and differentiation of MSCs cultivated in microscaffold, cell culture medium, FBS, and phosphate-buffered saline (PBS) were purchased from Lonza (Basel, Switzerland). Cell culture plates were obtained from Corning Life Science, Inc. (Acton, MA, USA). Cell Trace Far Red, AlamarBlue, 4′,6-diamidino-2-phenylindole (DAPI) mounting medium and insulin-transferrin-selenium (ITS) were provided by Life Technology (Carlsbad, CA, USA). TGF-β1 was purchased from Bio Vision Inc. (Milpitas, CA, USA). Dexamethasone, L-ascorbic acid-2-phosphate, sodium pyruvate, L-proline and Alcian blue were supplied by Sigma-Aldrich, and optical cutting temperature (OCT) compound was obtained from Leica Biosystems Inc. (Richmond, IL, USA).

MSC Culture on the Magnetically Actuated Microscaffold: The PLGA microscaffolds and the MNP-attached microscaffolds were sterilized with 70% ethanol for 30 min and washed with PBS two times. Then, the scaffolds were transferred into the wells of an ultralow attachment 96-well plate at a density of ten scaffolds per well, and D1 mouse MSCs were seeded on the scaffolds at a density of 1×10^6 cells per well. The MSC-seeded scaffolds were cultured in a 5% CO_2 incubator at 37 °C, and the culture medium was replaced every 2 d.

MSC Proliferation, Viability, and Cell Differentiation Tests: To identify the cell distribution of the PLGA microscaffolds and the MNP-attached microscaffolds by confocal microscopy, the cytoplasms of MSCs were stained with 10 μg mL^{-1} Cell Trace Far Red before the seeding of the MSCs on the microscaffolds. After the seeding, the MSCs were cultured on the microscaffolds for an initial 5 d, after which the microscaffolds were fixed with 4% paraformaldehyde, embedded in compound, and frozen at −20 °C. Then, the microscaffolds were cryosectioned (10 μm in thickness) and counterstained with DAPI mounting medium to visualize the nuclei. The sectioned samples were then observed using a Leica SP5 confocal microscope. Quantitative evaluations of MSC proliferation and viability on the microscaffolds were performed using the AlamarBlue assay according to the manufacturer's protocol on days 3, 6, 9, and 12 after cell seeding.[50] Briefly, the microscaffolds containing the MSCs were washed with PBS and incubated with 10% AlamarBlue-supplemented Dulbecco modified eagle medium (DMEM) at 37 °C and 5% CO_2 for 24 h. Then, 200 μL of the medium was transferred to a 96-well plate to measure the fluorescence intensity on a microplate reader (Varioskan flash, Thermo Scientific, USA) at an excitation wavelength of 550 nm and an emission wavelength of 590 nm.

Chondrogenic MSC differentiation in the PLGA microscaffolds and the MNP-attached microscaffolds was achieved using chondrogenic medium, which consists of DMEM with 4.5 g mL^{-1} glucose, 1% ITS, 0.1×10^{-6} M dexamethasone, 50 μg mL^{-1} L-ascorbic acid-2-phosphate, 100 μg mL^{-1} sodium pyruvate, 40 μg mL^{-1} L-proline, and 10 μg mL^{-1} TGF-β1. To assess the chondrogenesis by histological and immunohistochemical analysis, at day 21, the microscaffolds containing the D1 MSCs were embedded in OCT compound and frozen at −20 °C. The frozen microscaffolds were cryosectioned (10 μm in thickness), stained with Alcian blue in 3% acetic acid (pH 2.5) (Sigma, USA) and observed in an inverted microscope (Eclipse Ti-U, Nikon, Japan). For immunohistochemistry, the cryosectioned microscaffolds were incubated with Anti-COL11A1 antibody (Abcam, UK) for 1 h at room temperature and followed by incubation with Goat Anti-Rabbit IgG H&L Alexa Fluor 594, as a secondary antibody (Abcam, UK). For qRT-PCR analysis, total RNAs were extracted from the microscaffolds using TaKaRa MiniBEST Universal RNA Extraction Kit (Takara, Japan), the reverse transcription (RT) using PrimeScript Master Mix (Takara, Japan), and then qRT-PCR was performed using 5× HOT FIREPol, EvaGreen, and qPCR Supermix (Solis BioDyne, Estonia).

Supporting Information

Supporting Information is available from the Wiley Online Library or from the author.

© 2017 WILEY-VCH Verlag GmbH & Co. KGaA, Weinheim

Acknowledgements

G.G. and J.H. contributed equally to this work. This work was supported by the Industrial Technology Innovation Program [10060059, Externally Actuatable Nanorobot System for Precise Targeting and Controlled Releasing of Drugs] funded by the Ministry of Trade, Industry and Energy (MOTIE, Korea). The authors are grateful to Prof. Jong-Keun Seon and Prof. Eun-Kyoo Song (Department of Orthopedic Surgery, Center for Joint Disease, Chonnam National University Hwasun Hospital) for providing the D1 cell lines.

Conflict of Interest

The authors declare no conflict of interest.

Keywords

articular cartilage repair, magnetic field, mesenchymal stem cells, porous scaffold beads

Received: December 1, 2016
Revised: March 15, 2017
Published online:

[1] C.-W. Ha, M. J. Noh, K. B. Choi, K. H. Lee, *Cytotherapy* **2012**, *14*, 247.
[2] M. Ondrésik, F. R. Azevedo Maia, A. da Silva Morais, A. C. Gertrudes, A. H. Dias Bacelar, C. Correia, C. Gonçalves, H. Radhouani, R. Amandi Sousa, J. M. Oliveira, R. L. Reis, *Biotechnol. Bioeng.* **2017**, *114*, 717.
[3] S. Marlovits, P. Zeller, P. Singer, C. Resinger, V. Vécsei, *Eur. J. Radiol.* **2006**, *57*, 24.
[4] U. Noth, A. F. Steinert, R. S. Tuan, *Nat. Clin. Pract. Rheumatol.* **2008**, *4*, 371.
[5] B. D. Smith, D. A. Grande, *Nat. Rev. Rheumatol.* **2015**, *11*, 213.
[6] T. Ogura, A. Tsuchiya, S. Mizuno, *Orthop. Res. Rev.* **2015**, *7*, 1.
[7] T. Kusano, R. P. Jakob, E. Gautier, R. A. Magnussen, H. Hoogewoud, M. Jacobi, *Knee Surg. Sports Traumatol. Arthrosc.* **2012**, *20*, 2109.
[8] P. C. Kreuz, S. Müller, U. Freymann, C. Erggelet, P. Niemeyer, C. Kaps, A. Hirschmüller, *Am. J. Sport. Med.* **2011**, *39*, 1697.
[9] S. E. Kim, J. H. Park, Y. W. Cho, H. Chung, S. Y. Jeong, E. B. Lee, I. C. Kwon, *J. Controlled Release* **2003**, *91*, 365.
[10] T. K. Kim, J. J. Yoon, D. S. Lee, T. G. Park, *Biomaterials* **2006**, *27*, 152.
[11] S.-W. Choi, Y.-C. Yeh, Y. Zhang, H.-W. Sung, Y. Xia, *Small* **2010**, *6*, 1492.
[12] S. M. Lim, H. J. Lee, S. H. Oh, J. M. Kim, J. H. Lee, *J. Biomed. Mater. Res., Part B* **2009**, *90*, 521.
[13] C. Perka, O. Schultz, R.-S. Spitzer, K. Lindenhayn, G.-R. Burmester, M. Sittinger, *Biomaterials* **2000**, *21*, 1145.
[14] S.-W. Choi, Y. Zhang, Y.-C. Yeh, A. Lake Wooten, Y. Xia, *J. Mater. Chem.* **2012**, *22*, 11442.
[15] N. Luciani, V. Du, F. Gazeau, A. Richert, D. Letourneur, C. Le Visage, C. Wilhelm, *Acta Biomater.* **2016**, *37*, 101.
[16] J. Hori, M. Deie, T. Kobayashi, Y. Yasunaga, S. Kawamata, M. Ochi, *J. Orthop. Res.* **2011**, *29*, 531.
[17] Y. Qi, Z. Yang, Q. Ding, T. Zhao, Z. Huang, G. Feng, *Exp. Ther. Med.* **2016**, *11*, 458.
[18] E. E. Mahmoud, G. Kamei, Y. Harada, R. Shimizu, N. Kamei, N. Adachi, N. A. Misk, M. Ochi, *Cell Transplant.* **2016**, *25*, 1073.
[19] S. Panseri, A. Russo, M. Sartori, G. Giavaresi, M. Sandri, M. Fini, M. C. Maltarello, T. Shelyakova, A. Ortolani, A. Visani, V. Dediu, A. Tampieri, M. Marcacci, *Bone* **2013**, *56*, 432.
[20] A. Ito, Y. Takizawa, H. Honda, K. I. Hata, H. Kagami, M. Ueda, T. Kobayashi, *Tissue Eng.* **2004**, *10*, 833.
[21] M. Mahmoudi, S. Sant, B. Wang, S. Laurent, T. Sen, *Adv. Drug Delivery Rev.* **2011**, *63*, 24.
[22] H. Glickstein, R. B. El, G. Link, W. Breuer, A. M. Konijn, C. Hershko, H. Nick, Z. I. Cabantchik, *Blood* **2006**, *108*, 3195.
[23] E. H. Jebens, M. E. Monk-Jones, *Bone Joint J.* **1959**, *41*, 388.
[24] D. Choudhury, R. Walker, T. Roy, S. Paul, R. Mootanah, *Int. J. Precis. Eng. Manuf.* **2013**, *14*, 1847.
[25] K. J. Doege, M. Sasaki, T. Kimura, Y. Yamada, *J. Biol. Chem.* **1991**, *266*, 894.
[26] A. Shafiee, M. Soleimani, G. A. Chamheidari, E. Seyedjafari, M. Dodel, A. Atashi, Y. Gheisari, *J. Biomed. Mater Res., Part A.* **2011**, *99*, 467.
[27] M. Ullah, H. Hamouda, S. Stich, M. Sittinger, J. Ringe, *BioRes. Open Access* **2012**, *6*, 297.
[28] S. Floyd, C. Pawashe, M. Sitti, *IEEE Trans. Robot.* **2009**, *25*, 1332.
[29] S. Karkabi, N. Rosenberg, *Open J. Clin. Diagn.* **2015**, *5*, 68.
[30] H.-W. Tung, D. F. Sargent, B. J. Nelson, *J. Appl. Crystallogr.* **2014**, *47*, 692.
[31] D. F. Young, B. R. Munson, T. H. Okiishi, W. W. Huebsch, *A Brief Introduction to Fluid Mechanics*, Wiley, Hoboken, NJ, **2010**.
[32] H. Gao, W. Shi, L. B. Freund, *Proc. Natl. Acad. Sci. USA* **2005**, *102*, 9469.
[33] S. Mura, H. Hillaireau, J. Nicolas, B. Le Droumaguet, C. Gueutin, S. Zanna, N. Tsapis, E. Fattal, *Int. J. Nanomed.* **2011**, *6*, 2591.
[34] M. D. Krebs, K. A. Sutter, A. S. Lin, R. E. Guldberg, E. Alsberg, *Acta Biomater.* **2009**, *5*, 2847.
[35] T. K. Kim, J. J. Yoon, D. S. Lee, T. G. Park, *Biomaterials* **2006**, *27*, 152.
[36] A. R. Vancha, S. Govindaraju, K. V. Parsa, M. Jasti, M. González-García, R. P. Ballestero, *BMC Biotechnol.* **2004**, *4*, 1.
[37] H. Li, Z. Jin, S. Cho, S. Y. Ko, J.-O. Park, S. Park, *Int. Conf. on Ubiquitous Robots and Ambient Intelligence*, IEEE, Xian, China, **2016**, pp. 466.
[38] A. Elias, A. Tsourkas, *ASH Annual Meeting and Exposition*, American Society of Hematology, San Diego, California, USA, **2009**, pp. 720.
[39] N. Singh, G. J. Jenkins, R. Asadi, S. H. Doak, *Nano Rev. Exp.* **2010**, *1*, 1.
[40] E. A. Makris, A. H. Gomoll, K. N. Malizos, J. C. Hu, K. A. Athanasiou, *Nat. Rev. Rheumatol.* **2015**, *11*, 21.
[41] E. N. Blaney Davidson, E. L. Vitters, W. B. van den Berg, P. M. van der Kraan, *Arthritis Res. Ther.* **2006**, *8*, 1.
[42] H. Koga, L. Engebretsen, J. E. Brinchmann, T. Muneta, I. Sekiya, *Knee Surg. Sports Traumatol. Arthrosc.* **2009**, *17*, 1289.
[43] F. Mwale, P. L. Girard-Lauriault, H. T. Wang, S. Lerouge, J. Antoniou, M. R. Wertheimer, *Tissue Eng.* **2006**, *12*, 2639.
[44] A. Nazempour, B. J. Van Wie, *Ann. Biomed. Eng.* **2016**, *44*, 1325.
[45] K. M. Hubka, R. L. Dahlin, V. V. Meretoja, F. K. Kasper, A. G. Mikos, *Tissue Eng., Part B* **2014**, *20*, 641.
[46] S. Stolfa, M. Skorvanek, P. Stolfa, J. Rosocha, G. Vasko, J. Sabo, *Physiol. Res.* **2007**, *56*, S45.
[47] H. D. Amin, M. A. Brady, J.-P. St-Pierre, M. M. Stevens, D. R. Overby, C. R. Ethier, *Tissue Eng., Part A* **2014**, *20*, 1612.
[48] M. P. Kummer, J. J. Abbott, B. E. Kratochvil, R. Borer, A. Sengul, B. J. Nelson, *IEEE Trans. Robot.* **2010**, *26*, 1006.
[49] E. Diller, J. Giltinan, M. Sitti, *Int. J. Robot. Res.* **2013**, *32*, 614.
[50] R. C. Squatrito, J. P. Connor, R. E. Buller, *Gynecol. Oncol.* **1995**, *58*, 101.

© 2017 WILEY-VCH Verlag GmbH & Co. KGaA, Weinheim